

QCD Corrections to Diboson Production¹

J. Ohnemus

*Department of Physics
University of California
Davis, CA 95616*

Abstract

The QCD radiative corrections to hadronic diboson production are reviewed. The radiative corrections for $W^\pm\gamma$, $Z\gamma$, ZZ , W^+W^- , and $W^\pm Z$ are discussed. Similarities and differences in the behavior of the order α_s cross sections for these processes are emphasized.

Introduction

The production of weak boson pairs is an important topic to study at hadron colliders because these processes can be used to test the standard model (SM) as well as probe beyond it [1]. Diboson production is important for the following reasons.

- The $W^\pm\gamma$, $W^\pm Z$, and W^+W^- processes can be used to test the trilinear $WW\gamma$ and WWZ couplings. These couplings are completely fixed by the $SU(2) \otimes U(1)$ gauge structure of the SM, thus measurements of these couplings provide stringent tests of the SM. Remarkable progress has recently been made in measuring these couplings at the Fermilab Tevatron collider [2].
- The electroweak symmetry breaking (EWSB) mechanism can be probed by studying weak boson pair production. The EWSB mechanism is unknown, but it is believed that either there exists a scalar particle with mass $m < 1$ TeV or else the longitudinal components of the W and Z bosons become strongly interacting for parton center-of-mass energies larger than about 1 TeV [3]. For example, the observation of resonance production of ZZ , W^+W^- , or $\gamma\gamma$ would be a signal for the standard model Higgs boson, whereas enhanced production of longitudinally polarized W and Z pairs would be evidence for a strongly interacting EWSB scenario.
- Diboson production is a potential background to new physics. New heavy particles, such as H^0 , H^\pm , ρ_{TC} , η_{TC} , W' , Z' , \tilde{q} , and \tilde{g} can decay into weak boson pairs.

¹Contribution to the Proceedings of the International Symposium on Vector Boson Self-Interactions, UCLA, Feb. 1-3, 1995.

In order to test and probe the SM with hadronic diboson production, it is necessary to have precise calculations of SM diboson production, which means the cross sections must be calculated to next-to-leading-order (NLO). The NLO cross section is, in general, less sensitive to the choices of the arbitrary factorization and renormalization scales.

The results described here are based on complete $\mathcal{O}(\alpha_s)$ calculations of the processes $p\bar{p} \rightarrow V_1 V_2 + X$ where $V_i = W, Z, \gamma$ [4]. The calculations also include the leptonic decays of the W and Z bosons [5, 6]. This is an important feature to include since the W and Z bosons are observed experimentally via their leptonic decay products. It is therefore important to include the experimental cuts on the decay leptons when comparing a theoretical calculation to the experimental data.

The calculations have been done using a combination of analytic and Monte Carlo integration techniques. Among the advantages of this formalism are:

- It is easy to impose cuts in the calculation.
- It is possible to calculate any number of observables simultaneously by simply histogramming the quantity of interest.
- It is possible to calculate not only the NLO inclusive cross section, but also the 0-jet and 1-jet exclusive cross sections.

Details of the formalism can be found in the original references [4, 5, 6].

The $Z\gamma$ and $W\gamma$ Processes

The first processes to be considered are the $Z\gamma$ and $W\gamma$ processes. The total LO and NLO cross sections for these processes are plotted as functions of the center of mass energy in Fig. 1. The difference between the NLO and LO curves is the $\mathcal{O}(\alpha_s)$ correction. In the $Z\gamma$ process, the $\mathcal{O}(\alpha_s)$ corrections range from 10% to 30% over the domain of \sqrt{s} . This is what one naively expects since α_s is of order 0.10. In the $W\gamma$ process, on the other hand, the corrections range from 20% at small \sqrt{s} to a surprising 300% at large \sqrt{s} .

In order to understand the large $\mathcal{O}(\alpha_s)$ corrections in the $W\gamma$ process, it is instructive to compare the behavior of the $2 \rightarrow 2$ and $2 \rightarrow 3$ processes for $Z\gamma$ and $W\gamma$ production. Figure 2(a) compares the $2 \rightarrow 2$ cross sections. Normally, hadronic W production is about twice as large as hadronic Z production because the W -to-quark coupling is about twice as big as the Z -to-quark coupling. However, for the $W\gamma$ and $Z\gamma$ processes, exactly the opposite behavior is seen; the $W\gamma$ cross section is only half as big as the $Z\gamma$ cross section. The $W\gamma$ cross section is smaller because it is suppressed by a radiation amplitude zero (RAZ) [7]. Delicate cancellations in the $W^\pm\gamma$ amplitude cause it to vanish at $\cos\theta^* = \pm\frac{1}{3}$ where θ^* is the parton center-of-mass scattering angle.

The $2 \rightarrow 3$ cross sections for $W\gamma$ and $Z\gamma$ are compared in Fig. 2(b). Here a jet is defined as a final state quark or gluon with transverse momentum $p_T > 50$ GeV and pseudorapidity $|\eta| < 3$. The cross sections have been decomposed into contributions from qg and $q\bar{q}$ initial states (qg also includes $\bar{q}g$). The $qg \rightarrow W\gamma + 1$ jet cross section is about twice as big as the $qg \rightarrow Z\gamma + 1$ jet cross section, as naively expected. (The $qg \rightarrow W\gamma q$ subprocess does not

have a RAZ.) The $q\bar{q} \rightarrow W\gamma + 1 \text{ jet}$ and $q\bar{q} \rightarrow Z\gamma + 1 \text{ jet}$ cross sections, on the other hand, are nearly equal, indicating that the former is still suppressed relative to the later. (The $q\bar{q} \rightarrow W\gamma g$ subprocess has a RAZ in the limit $E_g \rightarrow 0$.)

In summary, the $2 \rightarrow 2$ $W\gamma$ cross section is suppressed relative to the $2 \rightarrow 2$ $Z\gamma$ cross section by a RAZ, while the $2 \rightarrow 3$ $W\gamma$ cross section is larger than the $2 \rightarrow 3$ $Z\gamma$ cross section due to the larger W -to-quark coupling. The net result of these two behaviors is that the $\mathcal{O}(\alpha_s)$ corrections are much larger for $W\gamma$ production than for $Z\gamma$ production.

Figure 3 again shows the total $Z\gamma$ and $W\gamma$ cross sections versus \sqrt{s} , but now the NLO cross sections have been decomposed into the Born cross sections and $\mathcal{O}(\alpha_s)$ corrections from $q\bar{q}$ and qg initial states. This decomposition shows that the $\mathcal{O}(\alpha_s)$ $q\bar{q}$ corrections tend to be proportional to the Born cross section, whereas the $\mathcal{O}(\alpha_s)$ qg corrections increase rapidly with \sqrt{s} . The $\mathcal{O}(\alpha_s)$ qg corrections increase with \sqrt{s} because the gluon density increases with \sqrt{s} .

Figure 4 shows the $p_T(\gamma)$ spectra for $Z\gamma$ and $W^+\gamma$ production at the Large Hadron Collider (LHC) center of mass energy ($\sqrt{s} = 14 \text{ TeV}$). The figure shows that the NLO corrections increase with $p_T(\gamma)$. This behavior is common to all the diboson processes; the NLO corrections increase with the p_T of the boson.

The rapidity distribution of the photon in the diboson rest frame is shown in Fig. 5 for the Tevatron center of mass energy ($\sqrt{s} = 1.8 \text{ TeV}$). For the $Z\gamma$ process, the distribution exhibits the usual bell-shaped rapidity distribution, however, for the $W\gamma$ process, the distribution has a pronounced dip in the central rapidity region. This dip is due to the RAZ in the $W\gamma$ process. At the Tevatron energy, the NLO corrections slightly fill the dip, but do not obscure it. Figure 6 shows the photon rapidity distribution at the LHC energy. The NLO corrections are now very large in the $W\gamma$ process and they completely fill the dip in the central rapidity region. It may still be possible, however, to observe the dip in the $W\gamma + 1 \text{ jet}$ exclusive cross section [6].

Figure 7 compares the $p_T(\gamma)$ spectra for the $Z\gamma$ and $W\gamma$ processes at the Tevatron energy. This comparison shows that at high $p_T(\gamma)$, the $W\gamma$ distribution falls more rapidly than the $Z\gamma$ distribution. This behavior is also due to the RAZ in the $W\gamma$ process.

The ZZ , W^+W^- , and WZ Processes

Attention now turns to the ZZ , W^+W^- , and WZ processes. The transverse momentum distributions for these processes are shown in Fig. 8. The figure shows that the NLO corrections increase with the p_T of the weak boson and are quite large at high values of p_T . Also note that the NLO corrections increase in the order ZZ , W^+W^- , WZ . This behavior will be discussed later.

Figure 9 again shows the p_T spectra of the weak bosons, but now the 0-jet and 1-jet exclusive components of the NLO inclusive cross section are also shown. (The 0-jet and 1-jet exclusive cross sections sum to the NLO inclusive cross section.) This decomposition shows that the bulk of the large corrections at high p_T are due to events containing a hard jet in the final state. The jet definition used here is $p_T(\text{jet}) > 50 \text{ GeV}$ and $|\eta(\text{jet})| < 3$.

The large enhancements to the cross section at high p_T can be traced to collinear splittings in diagrams such as $qg \rightarrow Zq$ followed by $q \rightarrow qW$; the Z and the quark are produced with

high p_T and the quark subsequently radiates a nearly collinear W . In the collinear limit, the $qg \rightarrow WZq$ subprocess can be approximated by [8]

$$d\sigma(qg \rightarrow WZq) \approx d\sigma(qg \rightarrow Zq) \frac{g^2}{16\pi^2} \log^2 \left(\frac{p_T^2(Z)}{M_W^2} \right). \quad (1)$$

Figure 10 compares this collinear approximation to the full NLO calculation and shows that the approximation describes well the shape of the p_T distribution at high p_T .

The scale dependance of the total WZ cross section is illustrated in Fig. 11. A common scale Q has been used for both the renormalization scale μ and the factorization scale M . The Born and NLO inclusive cross sections are shown along with the 0-jet and 1-jet components of the NLO inclusive cross section. The 1-jet cross section is a LO quantity and thus has considerable scale dependance. The 0-jet cross section, on the other hand, is a NLO quantity and exhibits little scale dependance. The decomposition shows that the scale dependance of the NLO inclusive cross section is dominated by the scale dependance of the 1-jet component.

Figure 12 compares the p_T spectra of the weak bosons for the ZZ , W^+W^- , and WZ processes. The ZZ and W^+W^- distributions have the same shape at high p_T and are parallel to one another, whereas the WZ distribution falls more rapidly. A similar behavior was observed earlier in Fig. 7 where the $Z\gamma$ and $W\gamma$ processes were compared. In the present case, the WZ p_T spectrum falls faster than the ZZ and W^+W^- spectra because of an approximate amplitude zero [9] in the WZ process.

Approximate Amplitude Zero

The $q_1\bar{q}_2 \rightarrow WZ$ subprocess is very similar to the $q_1\bar{q}_2 \rightarrow W\gamma$ subprocess, in fact, they are described by the same set of Feynman diagrams, with Z and γ interchanged. Recall that the RAZ in the $W\gamma$ process gave rise to a large $\mathcal{O}(\alpha_s)$ correction. A difference between the two processes is that whereas the $W^\pm\gamma$ process has an exact amplitude zero at $\cos\theta^* = \pm\frac{1}{3}$, the $W^\pm Z$ process has only an approximate amplitude zero at $\cos\theta^* = \pm 0.1$. Basically, what happens in the WZ case is that the dominant helicity amplitudes have an exact zero, while the other helicity amplitudes remain finite but small. The approximate amplitude zero in the WZ process causes the NLO corrections to be larger than they were in either the ZZ or W^+W^- processes. The approximate amplitude zero suppresses the WZ Born cross section and thus makes the NLO corrections appear large. A more in depth discussion of approximate amplitude zeros can be found in the talk by T. Han [10].

Summary

The QCD radiative corrections to weak boson pair production at hadron colliders has been reviewed. The $\mathcal{O}(\alpha_s)$ cross sections for the diboson combinations $Z\gamma$, $W\gamma$, ZZ , W^+W^- , and WZ have been discussed and compared. Some general features of the $\mathcal{O}(\alpha_s)$ cross sections are summarized here.

- The NLO corrections increase with the center-of-mass energy. This is due to the opening of the $qg \rightarrow V_1 V_2 q$ subprocess at $\mathcal{O}(\alpha_s)$ in conjunction with the gluon density which increases with the center-of-mass energy.

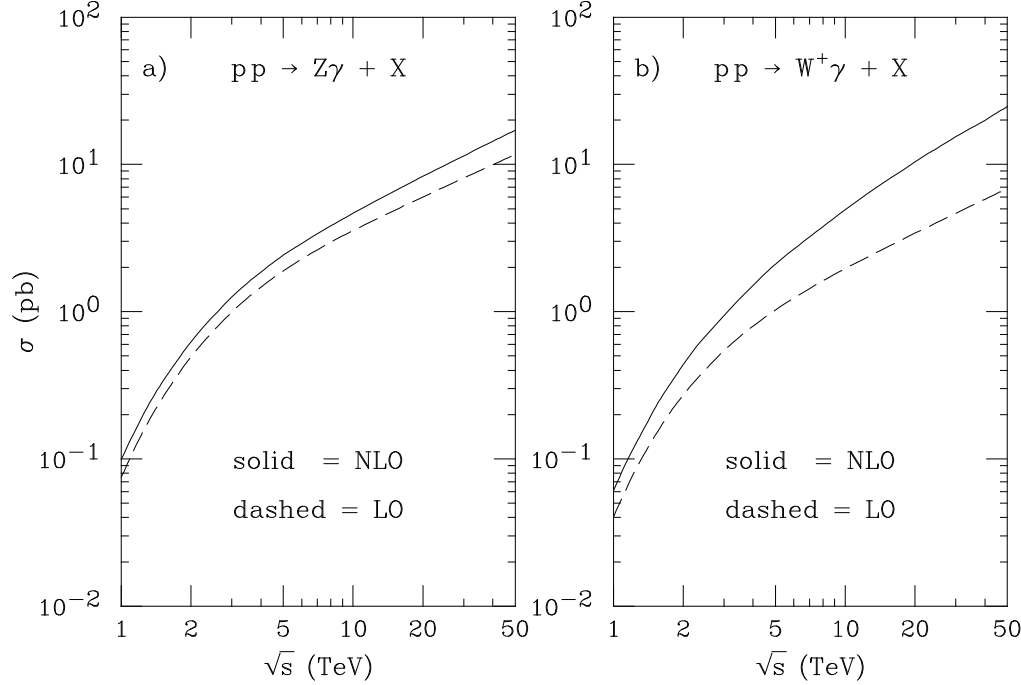


Figure 1: Total cross section as a function of the center-of-mass energy for (a) $pp \rightarrow Z\gamma + X$ and (b) $pp \rightarrow W^+\gamma + X$. The LO and NLO cross sections are shown.

- The NLO corrections are largest at high $p_T(V)$. This is due to collinear splittings in the $qg \rightarrow V_1 V_2 q$ subprocesses which give rise to an enhancement factor $\log^2(p_T^2(V_1)/M_2^2)$.
- The bulk of the large corrections at high $p_T(V)$ come from events which contain a hard jet in the final state.
- p_T distributions are most affected by the NLO corrections. These distributions tend to be enhanced at large values of p_T .
- Invariant mass and angular distributions under go relatively little change in shape at NLO, instead, these distributions tend to be scaled up uniformly.
- The NLO corrections to $W\gamma$ production are large due to a radiation amplitude zero.
- The NLO corrections to WZ production are large due to an approximate amplitude zero.
- The NLO corrections are modest at the Tevatron center of mass energy but are significant at the LHC energy.

References

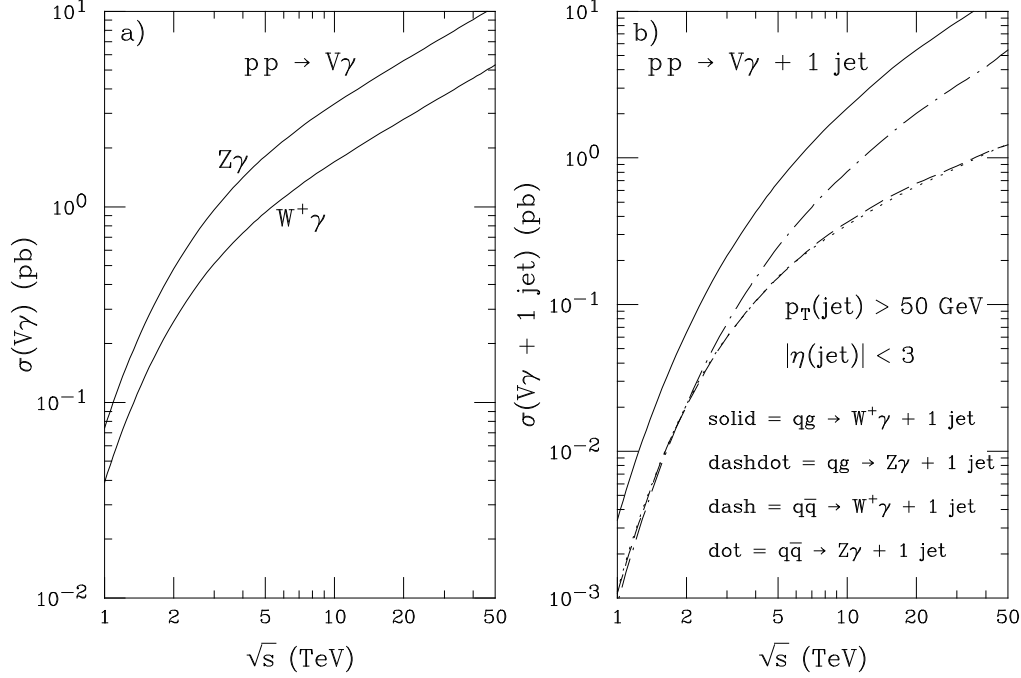


Figure 2: (a) The 2 → 2 Born cross sections for $pp \rightarrow Z\gamma$ and $pp \rightarrow W^+\gamma$. (b) The 2 → 3 cross sections for $Z\gamma$ and $W^+\gamma$ production. The cross sections have been decomposed into contributions from $q\bar{q}$ and qg initial states.

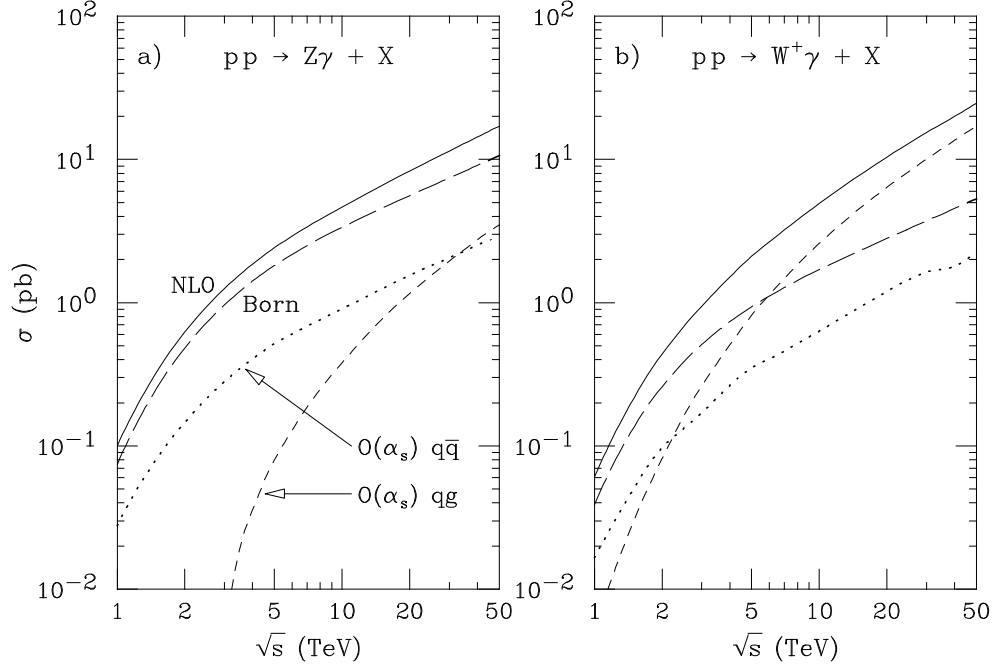


Figure 3: Same as Fig. 1, but now the NLO cross section has been decomposed into the Born cross section and the order α_s corrections from $q\bar{q}$ and qg initial states.

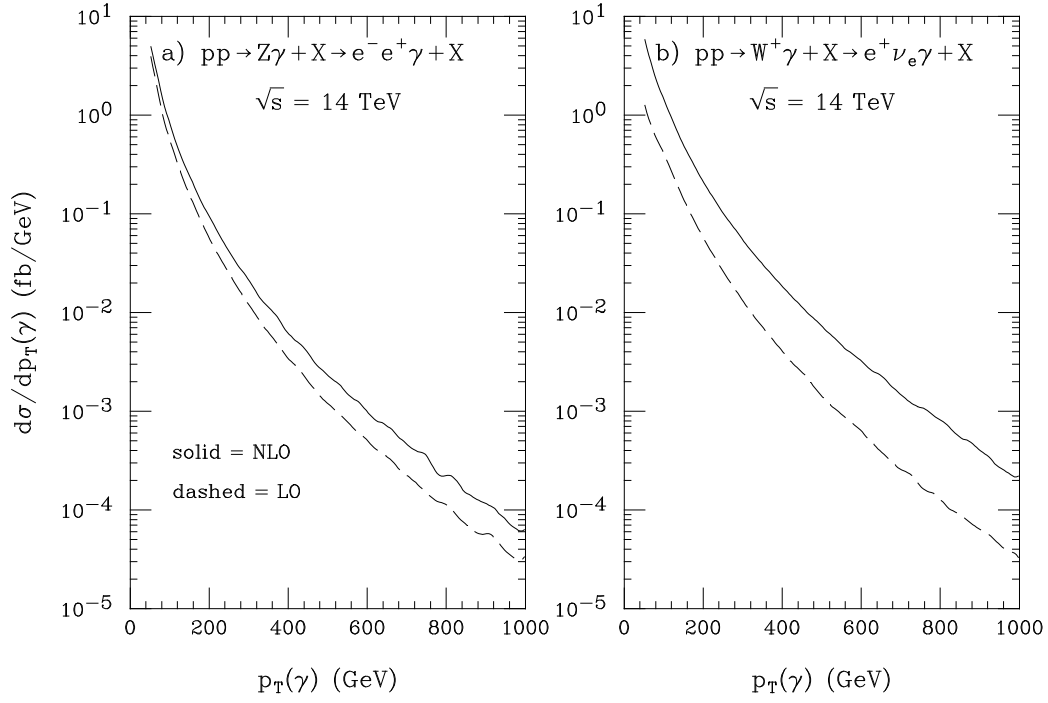


Figure 4: Photon transverse momentum distributions at the LHC energy for (a) $pp \rightarrow Z\gamma + X \rightarrow e^-e^+\gamma + X$ and (b) $pp \rightarrow W^+\gamma + X \rightarrow e^+\nu_e\gamma + X$.

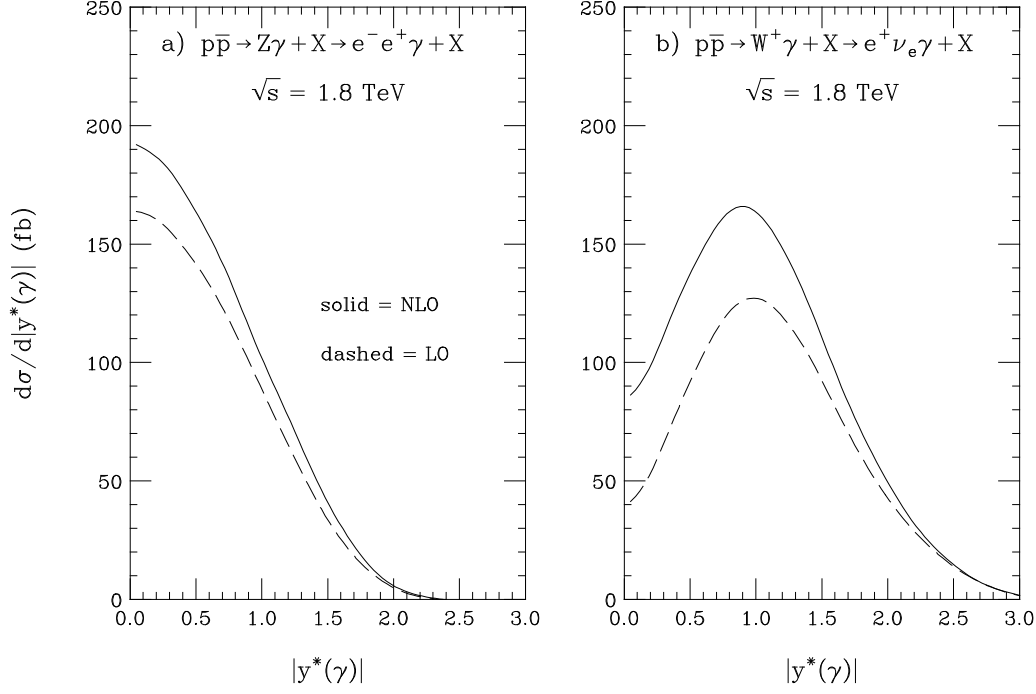


Figure 5: Photon rapidity distributions in the diboson rest frame at the Tevatron energy for (a) $Z\gamma$ production and (b) $W^+\gamma$ production.

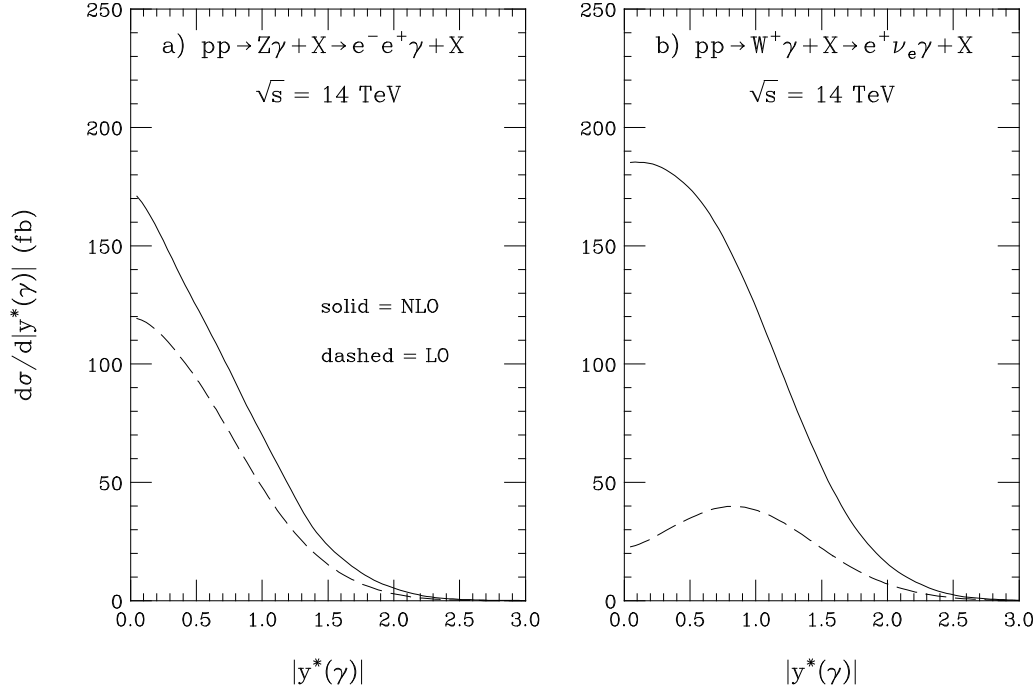


Figure 6: Same as Fig. 5, but for the LHC energy.

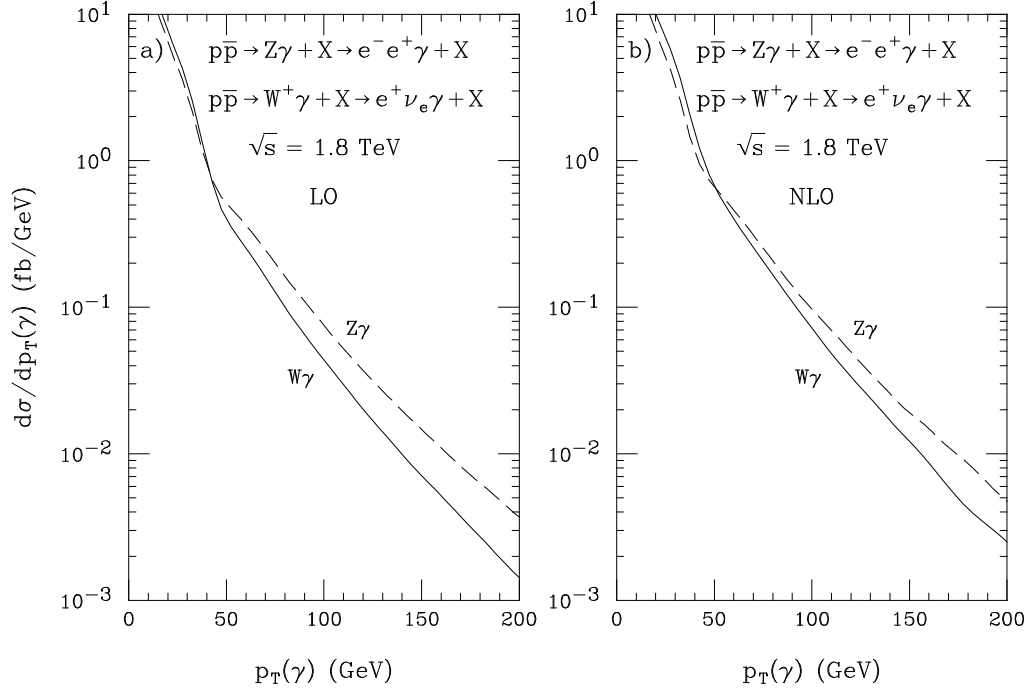


Figure 7: Photon transverse momentum distributions for $Z\gamma$ and $W\gamma$ production at the Tevatron energy. Parts (a) and (b) are the LO and NLO cross sections, respectively.

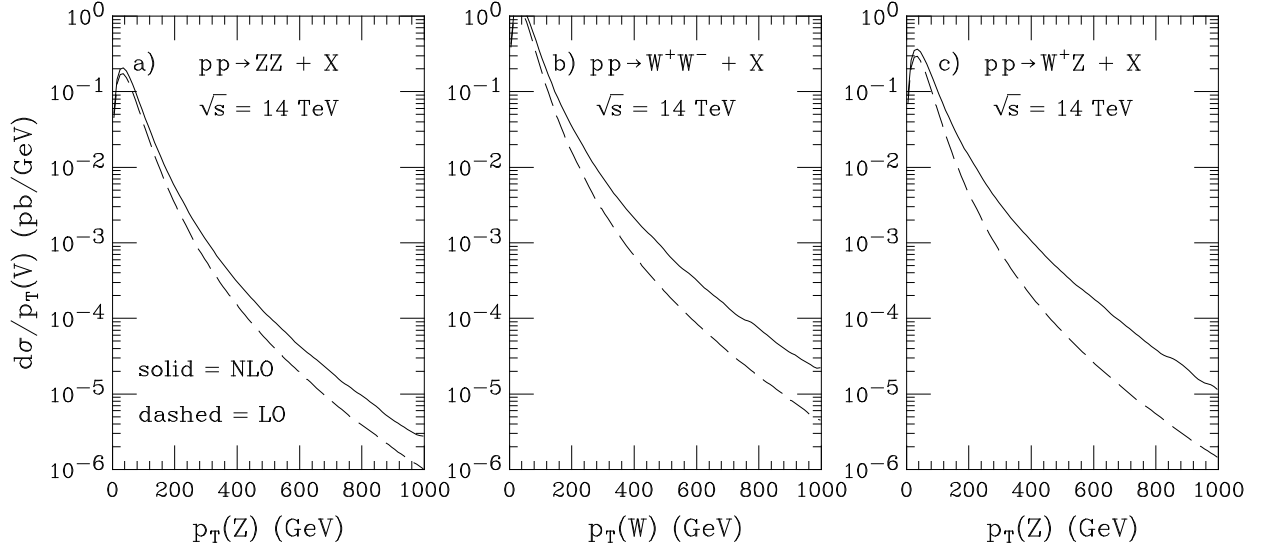


Figure 8: Weak boson transverse momentum distributions for (a) ZZ , (b) W^+W^- , and (c) W^+Z production at the LHC energy.

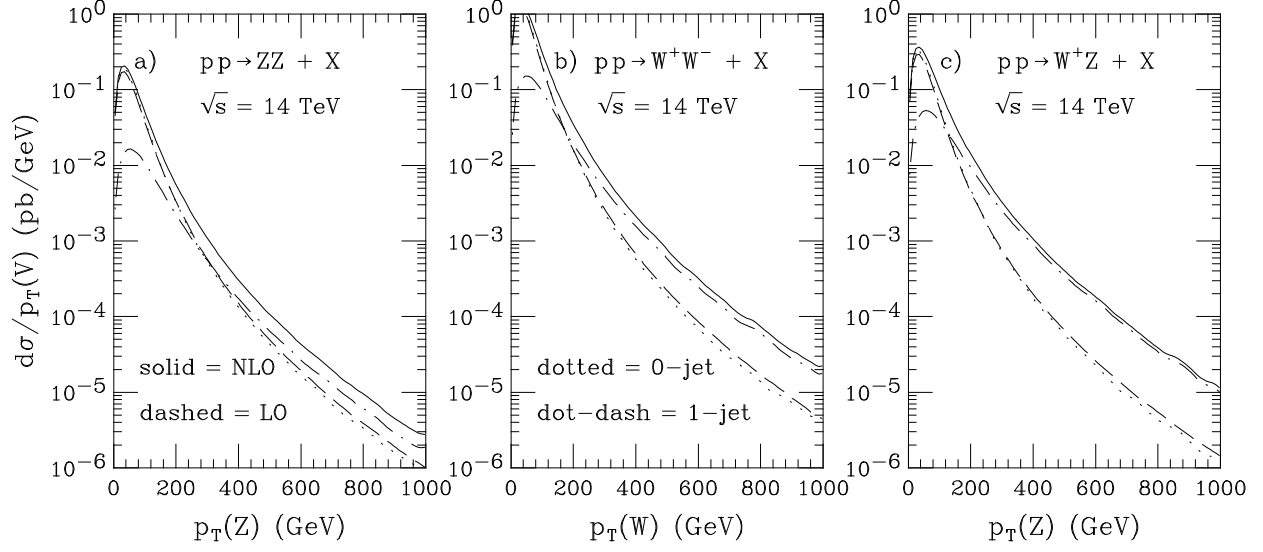


Figure 9: Same as Fig. 8. but now the 0-jet and 1-jet exclusive components of the NLO inclusive cross section are also shown.

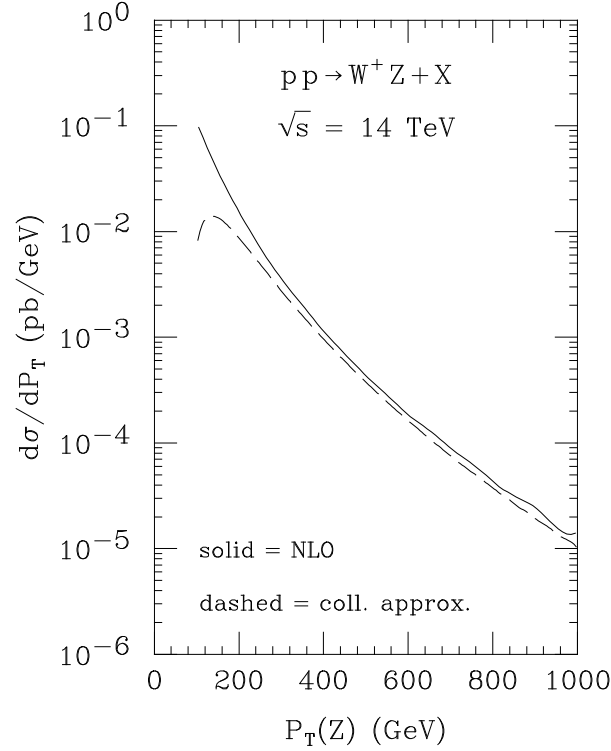


Figure 10: The $p_T(Z)$ distribution for $pp \rightarrow W^+Z + X$ at the LHC energy. The full NLO cross section is compared to the cross section obtained from the collinear approximation given in Eq. (1).

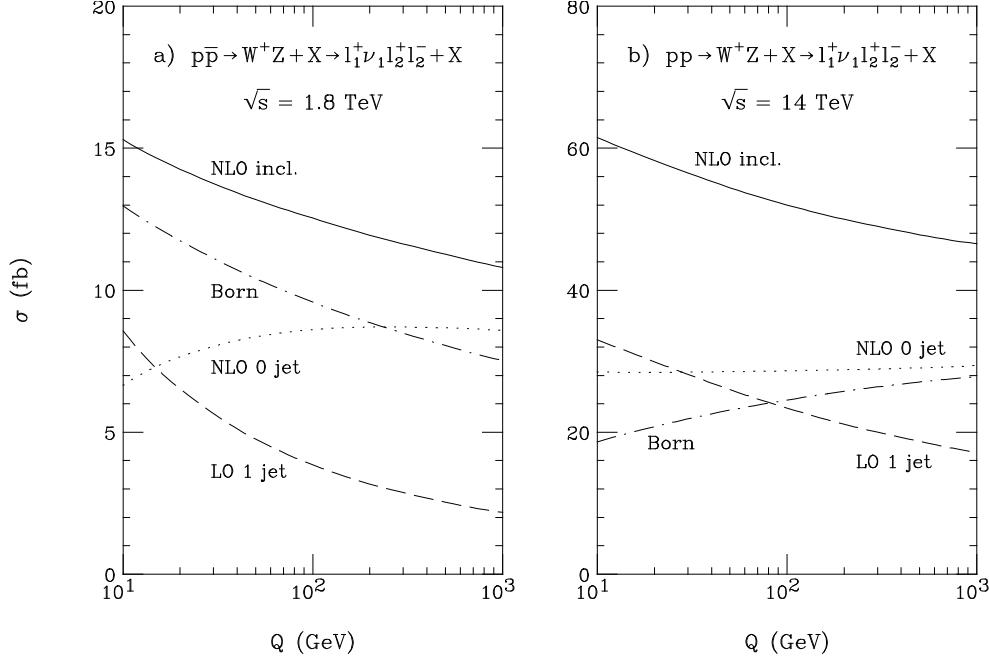


Figure 11: Total cross section for W^+Z production as a function of the scale Q for (a) the Tevatron energy and (b) the LHC energy. The Born, NLO inclusive, 0-jet exclusive, and 1-jet exclusive cross sections are shown.

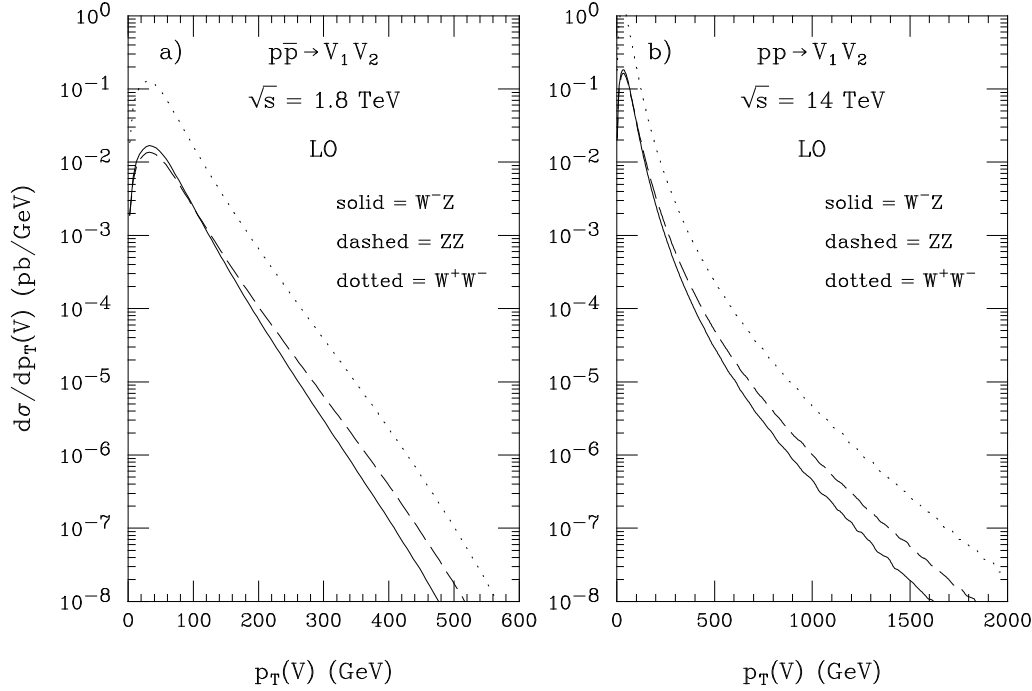


Figure 12: The weak boson transverse momentum distributions at LO for ZZ , W^+W^- , and W^-Z production. Parts (a) and (b) are for the Tevatron and LHC energies, respectively.

- [1] R.W. Brown and K.O. Mikaelian, Phys. Rev. D **19**, 922 (1979); R.W. Brown, K.O. Mikaelian, and D. Sahdev, *ibid.* **20**, 1164 (1979).
- [2] See talks by H. Aihara, T. Feuss, C. Wendt, H. Johari, L. Zhang, G. Landsberg, B. Wagner, and D. Neuberger in these proceedings.
- [3] D. Dicus and V. Mathur, Phys. Rev. D **7**, 3111 (1973); M. Veltman, Acta Phys. Pol. **B8**, 475 (1977); B.W. Lee, C. Quigg, and H. Thacker, Phys. Rev. D **16**, 1519 (1977); J. van der Bij and M. Veltman, Nucl. Phys. **B231**, 205 (1984); M. S. Chanowitz and M. K. Gaillard, Nucl. Phys. **B216**, 379 (1985).
- [4] J. Ohnemus and J.F. Owens, Phys. Rev. D **43**, 3626 (1991); J. Ohnemus, *ibid.* **44**, 1403 (1991); **44**, 3477 (1991); **47**, 940 (1993).
- [5] J. Ohnemus, Phys. Rev. D **50**, 1931 (1994); *ibid.* **51**, 1068 (1995).
- [6] U. Baur, T. Han, and J. Ohnemus, Phys. Rev. D **48**, 5140 (1993).
- [7] K.O. Mikaelian, M.A. Samuel, and D. Sahdev, Phys. Rev. Lett. **43**, 746 (1979); R.W. Brown, K.O. Mikaelian, and D. Sahdev Phys. Rev. D **20**, 1164 (1979); D. Zhu, Phys. Rev. D **22**, 2266 (1980); T.R. Grose and K.O. Mikaelian, Phys. Rev. D **23**, 123 (1981); C.J. Goebel, F. Halzen, and J.P. Leveille, Phys. Rev. D **23**, 2682 (1981); S.J. Brodsky and R.W. Brown, Phys. Rev. Lett. **49**, 966 (1982); M.A. Samuel, Phys. Rev. D **27**, 2724 (1983); R.W. Brown, K.L. Kowalski, and S.J. Brodsky, Phys. Rev. D **28**, 624 (1983); R.W. Brown and K.L. Kowalski, Phys. Rev. D **29**, 2100 (1984).
- [8] S. Frixione, P. Nason, and G. Ridolfi, Nucl. Phys. **B 383**, 3 (1992).
- [9] U. Baur, T. Han, and J. Ohnemus, Phys. Rev. Lett. **72**, 3941 (1994).
- [10] T. Han, in these proceedings.